RESEARCH PAPER

Investigating the Potential of Renewable-Hydrogen Energy Storage Systems (RHES) in Enabling Scotland's Farming Communities Net-Zero Transition and Sizing the Proposed RHES System

Haneen Al-Ali[1], Dallia Ali[1,*] and Ayatte I Atteya[1,2]

1 School of Engineering, Robert Gordon University, Scotland, UK
2 College of Engineering and Technology, Arab Academy for Science, Technology and Maritime Transport, Alexandria, Egypt
*Corresponding author. E-mail: d.ali@rgu.ac.uk

Citation
Haneen Al-Ali, Dallia Ali and Ayatte I Atteya (2023), Investigating the Potential of Renewable-Hydrogen Energy Storage Systems (RHES) in Enabling Scotland's Farming Communities Net-Zero Transition and Sizing the Proposed RHES System. *Green Energy and Environmental Technology* 2023(2), 1–32.

DOI
https://doi.org/10.5772/geet.16

Published
9 June 2023

Abstract

Renewable-hydrogen (H_2) is a key component in Scotland's decarbonisation plans and its implementation in farming communities can support achieving net-zero goals. HydroGlen, a demonstrative renewable-powered farming community at Glensaugh, is used as a case-study to investigate the potential of renewable-hydrogen in enabling Scotland farms' energy transition.
For our case-study farm, two renewable-hydrogen configurations (Solar-H_2 and Wind-H_2) were proposed, sized, and assessed to identify their capability in supplying most of the farm's residential and commercial demands by clean renewable-energy as well as the transport demands by green hydrogen stored during renewables' surplus. The effectiveness of the proposed configurations was then assessed against that of the Solar-Wind-H_2 configuration proposed by RINA (RINA 2021). The study started by assessing the currently installed renewables-system in meeting the farm's demands and results showed that the system can only meet 11% of farm's commercial and residential demands and none of the transport fuel demands. To allow meeting more residential and commercial demands as well as transport demands, a hybrid Solar-H_2 system was proposed with an additional photovoltaic (PV) capacity that was sized to feed a higher percentage of the demands with renewable power and a hydrogen energy-storage system to store the surplus in PV production in the form of green H_2 to be used in feeding the transport fuel demands. Components of the proposed green-H_2 energy-storage system (electrolyser and storage-tank) were accordingly sized. The effectiveness of the proposed hybrid PV-H_2 configuration was then assessed, and results showed it was capable of

supplying 35% of the residential and commercial demands from solar energy and 100% of the transport demands by green H_2. This generous amount of green H_2 resulted from the plenty PV daytime surplus given that most of the residential demand is not during sun availability hours.
A hybrid Wind-H_2 configuration was then proposed, sized and assessed. Results showed that this configuration was capable of supplying most of the residential and commercial demands from wind energy as the wind-generation profile closely matched these demands, and around 44% of transportation fuel demand by green H_2.
The levelized cost of energy (LCOE) was then estimated for each of the proposed hybrid configurations showing that the LCOE for the hybrid PV-H_2, 0.3 £/kWh, is more cost competitive than that of the Wind-H_2 of 0.4 £/kWh; thus, the hybrid PV-H_2 system was recommended for the farm.
Finally, a Simulink model was developed to simulate and assess the operation of the proposed PV-H_2 system given that this has not been considered in RINA study.

Keywords: solar energy systems, wind energy systems, hydrogen energy storage systems, modelling, sizing, LCOE

1. Introduction

The implementation of clean energy production from renewables is a key component towards achieving the net-zero target. However, given the intermittent nature of renewable energy systems (RES), energy storage is critical to mitigate this intermittency problem and realise the full potential of renewable energy. Energy storage devices can be classified according to a range of characteristics, including their storage capacity and duration, life expectancy, size, cost and safety, and environmental effect, including their recyclability [1]. There are numerous storage options; these include flow batteries which store energy directly in the electrolyte but are still in their infancy in terms of deployment, sodium-sulfur batteries which have a higher energy density than Li-ion batteries but have an inconvenient hot liquid metal electrolyte partially reducing the battery performance [2], supercapacitors which cannot provide electricity for an extended period of time, and compressed air and flywheels energy storage installations which are restricted by location requirements [3].

Hydrogen energy storage (HES) systems are distinguished from other types of renewable energy storage systems by their adaptability and capacity to deliver multiple services [4]. This quality is essential for grid operators to maintain system dependability and the integration of RES into the electricity, heating, and transportation infrastructures [4, 5]. Energy can be stored at large-scale using HES systems, ranging from 1 GWh to 1 TWh, whereas batteries generally range from

10 kWh to 10 MWh [5]. Fuel cell electric vehicles have additional hydrogen utilisation potential of interest [6]. The degree to which HES systems may enter energy storage markets will rely on a number of variables, including non-technological hurdles such as regulatory, safety, and economic concerns [7]. H_2 energy-storage is an emerging key enabler in Scotland's decarbonisation plans, and there is a need to demonstrate how its implementation can contribute to meeting the net-zero greenhouse gas (GHG) emission goals. Sizing the capacity of the HES system components needed with renewables and their economic viability represent key research components in assessing the potential of HES in enabling the clean energy transition. To this extent, many researchers have carried out valuable insights into sizing and assessing the feasibility of HES technologies for stand-alone and grid-connected hybrid renewable energy systems. Castaneda *et al.* [8] have investigated the sizing of HES system components within a stand-alone hybrid renewable-H_2 system using four different methods including: deterministic technique, MATLAB-based technical optimization method using Simulink Design Optimization (SDO) toolbox, and a techno-economic optimization using HOMER and iHOGA software, the results showed satisfaction of the load demand criteria while minimizing the total cost. In [9], a stand-alone PV-Fuel Cell (PV-FC) system has been sized using HOMER for supplying the electrical load demand of a remote village. The objective function was set to minimize the net present cost while maintaining the system reliability. The obtained results have shown that the optimal sizes of system components have achieved a minimal net present cost while satisfying the required load demand. It has been also observed that most of the annual energy produced was utilized for hydrogen generation, reflecting the potential of H_2 storage systems in absorbing the excess of renewable energy, thus decarbonizing the electrification of remote areas. The authors have also compared the results of the proposed stand-alone PV-FC system to a stand-alone PV-batteries system, and it was found that the former is better in terms of net present cost. Bernoosi and Nazari [10] have studied the feasibility of stand-alone PV-Fuel Cell Combined-Heat-and-Power (CHP) system for feeding both electrical and heating load demands. In this work, the contribution of HES has been assessed by studying the system with and without the use of H_2 storage technology, considering the integration of the proposed PV-FC system with batteries and domestic water heater to evaluate the total cost of the system. In each case, the sizes of PV-panels, batteries and water heater were determined, and the obtained results have shown corresponding reduction in the size of water heater and batteries with the use of H_2 storage system. Darei *et al.* [11] have studied the effect of increasing the size of H_2 electrolyser and fuel-cell on the production and planning of an energy system in Sweden involving rooftop PVs and CHP plants for serving district heating network and electricity demands. The study involved sizing and modelling the proposed H_2 system components and results have shown that increased capacities of electrolyser

and fuel-cell have contributed to great reduction in the grid energy purchase and production cost while increasing the heat recovery from H_2 system components and minimizing the load of CHP plants. Further research has been conducted for sizing Power-to-Gas (P2G) systems incorporating H_2 storage facilities for grid balancing services. Simonis and Newborough [12] have investigated the effect of multiple P2G configurations using different electrolyser capacities in conjunction with hydrogen storage buffers for capturing the excess of onshore wind energy in a German city and injecting it into the gas-grid. The study has been carried out based on predicting the excess of renewable electricity in the city during 2015–2020, with respect to the electricity and gas demand profiles. Results have indicated that upscaling the size of P2G system significantly increases the availability of hydrogen generation by electrolyser thus reducing wind curtailment scenarios in the considered region while increasing the contribution of green gas for balancing the gas-grid consumption. McDonagh *et al.* [13] have investigated multiple scenarios of integrating hydrogen P2G solutions with offshore wind farms from an investor perspective, considering different curtailment levels. A model has been developed to estimate the hourly generation and investor revenue of an offshore wind farm located in the Irish Sea in Ireland using the wind speed data and the electricity market price. Results have demonstrated that combining P2G installation with the considered wind farm allowed the most profitable configuration where the wind power is converted into hydrogen at lower energy rates and sold as electricity at higher energy rates. It has been concluded from the conducted literature that HES systems hold a great potential in decarbonizing multiple sectors, however sizing the capacity of HES systems, planning their operation and assessing their feasibility when integrated with renewables are key enablers for unlocking their full potential and promoting their large-scale development.

This paper investigates the potential of hybrid renewable-hydrogen energy storage systems in enabling the energy transition of Scotland's farms using Glensaugh farm as a case study for the investigation. At Glensaugh farm, just outside Fettercairn in Aberdeenshire, the HydroGlen Project aims turning the farm into a net-zero carbon emissions farm through feeding the farm's (electricity, heating, and transport) energy needs from a combination of renewable energy sources and on-site hydrogen production, compression, and storage [14]. Currently, Glensaugh farm has a renewable energy mix composed of a 50-kW wind turbine and 50 kW solar PV and is looking into installing more renewable capacity to meet all their residential, commercial, and transportation demands [14]. The farm's energy demands data and RINA feasibility report [14] have been provided by the James Hutton Institute (JHI).

This study started by evaluating the farm currently installed renewable system in meeting the farm's residential, commercial and transport demands. Based on this

evaluation, two hybrid renewable-H_2 systems were proposed. Option (1), a Hybrid Solar-H_2 system that utilizes the existing PV together with an extra grid-connected PV capacity that was sized to allow meeting more residential and commercial demands and a H_2 generator that was sized to allow storing the solar surplus in the form of green H_2 to be used for meeting the transport demands. The effectiveness of this proposed and sized hybrid PV-H_2 system was then assessed. For option (2), a hybrid Wind-H_2 system is proposed, sized and assessed. The proposed hybrid Wind-H_2 system utilizes the currently installed wind turbine as it was found capable of meeting most of the residential and commercial demands, together with a H_2 generator that was sized to allow storing the wind surplus in the form of green H_2 to be used for meeting the transport demands. The green H_2 produced in each of the proposed hybrid renewable-H_2 systems is utilized as fuel for meeting the farm transport demands rather than converting the H_2 back to electrical energy for 'on-grid' consumption because H_2 fuel is more competitively priced if it is marketed as a high-value gas [15]. The LCOE for each of the proposed hybrid configurations was estimated and they were compared to select the more cost-competitive option. Based on this comparison, a Simulink model was developed for the selected hybrid PV-H_2 system to assess in more detail its operation and potential.

2. *Evaluating Glensaugh Farm current operating renewable capacity*

Table 1 shows the data provided for the farm demands [14], where the transport demand is comprised of 12 vehicles accounting for 5110 kWh with no variation throughout the year. The currently installed renewable capacity comprises a mixture of a 50-kW solar PV and 50-kW wind turbine [14]. The on-site 50 kW wind turbine is not included in the calculations as it feeds directly into the national grid, not the farm demands. The RINA report proposes a new, 800 kW turbine to be installed for use in combination with the solar PV.

The energy output of the currently installed 50-kW PV system was calculated using the PVsyst software and results are shown in Table 2. The PVsyst includes extensive meteorological and PV system components databases that allows the user to select the PV system components (module and inverter) [16]. Based on the information provided by the farm owner, the PV and inverter modules were set in PVsyst to JC250M-24/Bb-v and SolarLake 15000-TL respectively, the tilt was set to 20°, and the azimuth, which is the direction the PV is facing, was set at 50°. From the PVsyst simulation results shown in Table 2, it was found that the annual energy output of the currently installed 50-kW solar system can only meet 11% of the residential and commercial total demand (40,316 kWh/364,330 kWh).

Table 1. Glensaugh Farm monthly load demand data in kWh [14].

Month	Residential monthly demand (kWh)	Commercial monthly demand (kWh)	Transport monthly demand (kWh)
January	6413	37,397	5110
February	6413	29,560	5110
March	6413	31,565	5110
April	5318	17,012	5110
May	4628	18,856	5110
June	3968	16,887	5110
July	3947	14,586	5110
August	4427	14,857	5110
September	5207	14,117	5110
October	6528	25,020	5110
November	6618	38,493	5110
December	7308	38,792	5110

Table 2. PVsyst Software' monthly energy output of Glensaugh Farm' currently installed PV system versus the farm's monthly residential and commercial total demand.

Month	Monthly residential and commercial total demand (kWh)	PVsyst simulation output monthly production from currently installed PV (kWh)
Jan	43,810	1,034
Feb	35,973	1,791
Mar	37,978	3,609
Apr	22,330	4,868
May	23,484	6,266
Jun	20,855	5,884
Jul	18,533	5,271
Aug	19,284	4,984
Sep	19,324	3,300
Oct	31,548	2,207
Nov	45,111	1,102
Dec	46,100	661
Total annual	364,330	40,316

3. Sizing the proposed PV-H_2 system

Given that the currently installed PV capacity is insufficient to meet the farm's energy demands alone without adding an 800 kW wind turbine as proposed by RINA's study [14], we here propose an alternative solution of extra PV capacity that allows meeting the farm's demands by 100% solar PV. The capacity of the proposed

PV system was accordingly sized, and its potential was assessed. A hydrogen energy storage system was also proposed and sized to store the excess in the PV production in the form of green hydrogen fuel to be used in clean fuelling of the farm's 12 vehicles. Figure 1 shows the proposed PV-H_2 Energy System.

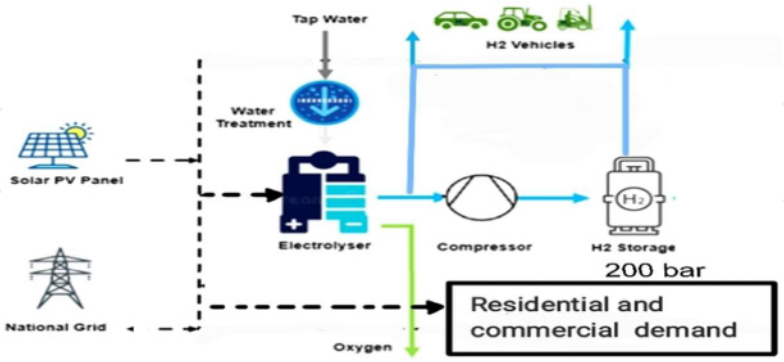

Figure 1. The proposed PV-H_2 system (source: adopted from [14]).

3.1. Sizing the new PV capacity

The size of the solar PV array that would be required for a grid-connected PV-H_2 system is calculated using Equation (1) [11]

$$\text{PV size} = \frac{\text{Monthly load demand in kWh}}{\text{PSH} * \text{Temperature losses} * \text{Inverter efficiency} * \text{Derate factor}} \quad (1)$$

where: the monthly load demand is taken as the sum of the farm's residential and commercial load demands in kWh. PSH is the geographic location monthly peak sun-hours calculated by taking the average values of three years based on Statista [17]. Derate factor refers to the system losses such as module power tolerance and wiring losses was taken as 0.774 [18]. Additional derate factors like temperature losses and inverter efficiency were taken as 0.88 and 0.96 respectively [18].

From the results of the 12-months calculated PV system sizes shown in Table 3, the required size of the new PV capacity is found to be 598 kW. Thus, in addition to the existing 50 kW solar capacity, an extra PV capacity of 548 kW is suggested to be installed in order to fully meet all energy requirements of the farm and community.

3.2. Sizing the electrolyser (H_2 generator) needed to store the new PV system energy surplus as green H_2

Given the high cost of electrolysers, it is desirable to maximise their utilisation [15]. Based on industrial standards, the electrolyser size is usually chosen to be between 20% and 40% of the PV capacity to increase the electrolyser's

Table 3. Sizing the PV capacity based on each month's load demand.

Month	Monthly load demand (kWh)	Average monthly peak sun-hours (PSH)	Temperature loss	Inverter efficiency	Derate factor	Monthly PV array size (kW)
January	43,810	48.1	0.88	0.96	0.774	1392
February	35,973	90.0	0.88	0.96	0.774	612
March	37,978	111.7	0.88	0.96	0.774	520
April	22,330	174.9	0.88	0.96	0.774	195
May	23,484	231.0	0.88	0.96	0.774	155
June	20,855	186.2	0.88	0.96	0.774	171
July	18,533	180.8	0.88	0.96	0.774	157
August	19,284	154.8	0.88	0.96	0.774	190
September	19,324	140.1	0.88	0.96	0.774	211
October	31,548	88.6	0.88	0.96	0.774	544
November	45,111	54.3	0.88	0.96	0.774	1270
December	46,100	40.0	0.88	0.96	0.774	1764

utilisation level. The possible downside is that there will be moments when total renewable generation surpasses the total electricity that the combined load and storage can absorb [15]. Selecting a 40% of the proposed 598 kW PV capacity suggests an electrolyser size of 239.2 kW. To allow better utilization, three units of 80 kW HySTAT 15–10 electrolysers from Hydrogenic manufacturer (highlighted in Figure 2) are accordingly selected.

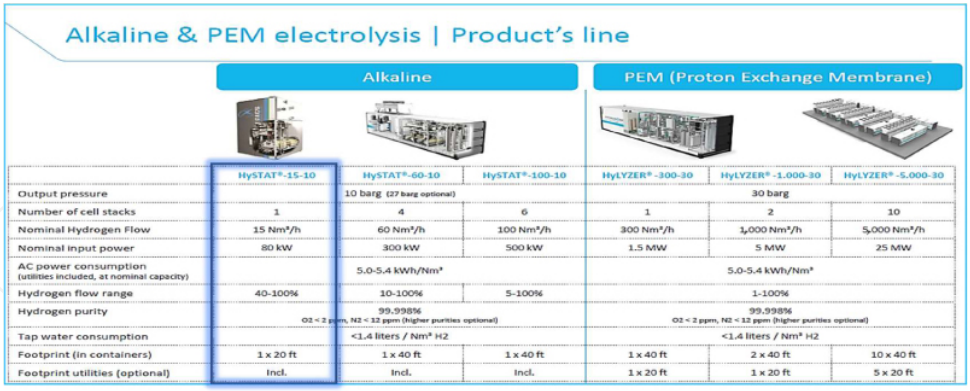

Figure 2. Hydrogenics electrolysis product lines [19].

3.3. Sizing the hydrogen storage tank

To identify the storage tank size, it is first necessary to identify the amount of H_2 produced by the electrolyser based on the surplus in the solar output from the proposed PV system. Using Pvsyst, the surplus in solar production was estimated by

comparing the monthly energy output of the newly sized PV capacity to the farm's total residential and commercial load demand. The monthly energy output of the PV system was estimated using the PVsyst software after setting the following inputs: the location was set to a Latitude of 57.20° N and a longitude of −2.20° E. PV Tilt angle was set as 37° after examining different tilt values to find the optimal, additionally Fordham [20] proved that the optimal tilt angle of a PV is equal to the site's latitude minus 20° thus in Scotland it is (57° − 20° = 37°). The azimuth was set at 0° as Scotland is in the northern hemisphere facing south. The PV module and inverter types were selected the same as the ones already installed on the farm, Figure 3 shows the system details. An optimized selection of inverter size is done by the PVsyst.

PV Array Characteristics

PV module		**Inverter**	
Manufacturer	Generic	Manufacturer	Generic
Model	JC250M-24/Bbv	Model	SolarLake 15000TL-PM
(Original PVsyst database)		(Original PVsyst database)	
Unit Nom. Power	250 Wp	Unit Nom. Power	15.0 kWac
Number of PV modules	2392 units	Number of inverters	31 units
Nominal (STC)	598 kWp	Total power	465 kWac
Modules	104 Strings x 23 In series	Operating voltage	400-850 V
At operating cond. (50°C)		Pnom ratio (DC:AC)	1.29
Pmpp	540 kWp		
U mpp	625 V		
I mpp	865 A		
Total PV power		**Total inverter power**	
Nominal (STC)	598 kWp	Total power	465 kWac
Total	2392 modules	Nb. of inverters	31 units
Module area	3891 m²	Pnom ratio	1.29
Cell area	3493 m²		

Figure 3. Specs. of the proposed 598 kW PV system.

Table 4 demonstrates the PVsyst simulation results showing the proposed PV system monthly DC energy output and the monthly AC solar energy excess which takes into account the inverter and wiring losses.

Based on the PV's monthly energy surplus, the amount of hydrogen produced monthly by the previously selected and sized electrolyser was calculated by dividing the PV energy excess by the electrolyzer energy consumption of 5.4 kWh/N m^3. The monthly hydrogen required for fuelling each vehicle in the farm was also calculated by using the 12 vehicles given total monthly consumption (5110 kWh) and the onboard H_2 fuel cell and sub-systems Round-trip efficiency (RTE) of 30% [21]. Given the RTE, the energy demand of the 12 vehicles becomes 17,033 kWh (5110/0.3), this equates to a monthly demand of 1419.4 kWh for each vehicle [14]. This amount is then converted from 1419.4 kWh to normal cubic meters (N m^3 of hydrogen) by multiplying it by the conversation factor 0.333 giving 473 N m^3 of H_2 required per month for each vehicle. This conversion factor was calculated based on the fact that at low heat value (LHV), 11.1 N m^3 of hydrogen is equivalent to 33.3 kWh [19]. Using the calculated monthly H_2 produced by electrolyser and the H_2 required by each

Table 4. PVsyst energy output simulation results for the 598 kW PV system.

Month	Monthly DC production from the proposed 598 kW PV system (kWh)	Monthly AC residential and commercial demand (kWh)	Monthly AC solar energy supplying the demand during the daytime (kWh)	Monthly AC solar energy excess (kWh)
January	19,740	43,810	7,850	11,450
February	29,900	35,970	9,630	19,660
March	54,040	37,980	14,220	38,790
April	65,220	22,330	10,960	53,020
May	82,320	23,480	13,240	67,540
June	74,280	20,860	12,600	60,250
July	73,070	18,530	11,090	60,560
August	63,230	19,280	10,070	51,950
September	54,020	19,320	8,680	44,300
October	32,920	31,580	10,030	22,200
November	19,340	45,110	9,010	9,880
December	13,740	46,100	6,610	6,770
Annual	**581,820**	**364,350**	**123,990**	**446,370**

vehicle, the number of vehicles that can be fed by clean green H_2 fuel every month was then calculated. The monthly accumulation of H_2 excess was then calculated and used in fuelling more vehicles. Finally, the residual monthly accumulated H_2 after feeding the farm 12 vehicles was calculated to be sold as a commodity or used in generating clean electricity. Results of all these calculations are shown in Table 5.

The volume of the H_2 storage tank was then determined based on the maximum amount of accumulated hydrogen, which is 30,058.7 N m^3. The volume of hydrogen can be lowered by employing a compressor. Using Boyles' law (Equation (2)), the new volume of hydrogen following compression with the temperature remaining constant is calculated.

$$P_1 V_1 = P_2 V_2 \quad (2)$$

where, P_1 is the pressure of H_2 output from the selected electrolyser; V_1 is the volume of the maximum accumulated H_2 (30,058.7 N m^3); P_2 is the pressure after compression; and V_2 is the volume after compression.

As specified in the HySTAT 15-10 electrolyser specifications, the hydrogen is supplied at a pressure P_1 = 10 bars. The pressure of the selected PURE ENERGY CENTER compressor P_2 is set to 200 bars [22]. Thus, using Equation (2), the volume of H_2 after compression will be:

$$V_2 = \frac{10 * 30{,}058.7}{200} = 1502.9 \text{ N } m^3.$$

Table 5. H_2 accumulation calculation results.

Month	Monthly excess in PV energy (kWh)	Electrolyser energy consumption (kWh/N m³)	Monthly H_2 Production (N m³)	One vehicle monthly H_2 consumption needs (N m³)	No of vehicles that can be supplied each month	Monthly H_2 excess after feeding the possible number of vehicles (N m³)	No of extra vehicles that can be supplied from the H_2 monthly accumulation	Monthly accumulated H_2 after feeding the farm's 12 vehicles (N m³)
Jan	11,450	5.4	2120.4	473	4	228.4	0	228.4
Feb	19,660	5.4	3640.7	473	7	329.7	1	85.1
Mar	38,790	5.4	7183.3	473	12	1507.3	0	1592.4
Apr	53,020	5.4	9818.5	473	12	4142.5	0	5735.0
May	67,540	5.4	12,507.4	473	12	6831.4	0	12,566.4
Jun	60,250	5.4	11,157.4	473	12	5481.4	0	18,047.8
Jul	60,560	5.4	11,214.8	473	12	5538.8	0	23,586.6
Aug	51,950	5.4	9620.4	473	12	3944.4	0	27,531.0
Sep	44,300	5.4	8203.7	473	12	2527.7	0	**30,058.7**
Oct	22,200	5.4	4111.1	473	8	327.1	4	28,493.8
Nov	9,880	5.4	1829.6	473	3	410.6	9	24,647.4
Dec	6,770	5.4	1253.7	473	2	307.7	10	20,225.1

Figure 4 illustrates the selected type of storage tank for this study: N5.0 (CP Grade H_2) Manifold cylinder pallet of maximum storage capacity 132 m³ and can store hydrogen at 200 bar [23]. To store the amount of H_2 accumulated, **12 storage tanks** (12 * 132 = 1584) are required, which accommodate any future expansion.

Figure 4. Hydrogen N5.0 (CP Grade H_2) manifolded cylinder pallet [23].

4. The Wind-H_2 system

A Wind-H_2 system, as illustrated in Figure 5, is proposed, sized and assessed as option (2). The RINA feasibility study (RINA 2021) identified that **an 800 kW**

Enercon E-53 with a 50 m hub height would be suitable for meeting the farm's demand. The sufficiency of this proposed wind turbine capacity in meeting the residential and commercial demands is therefore assessed, and based on the excess in the wind production, the best-suited hydrogen energy storage system was accordingly sized.

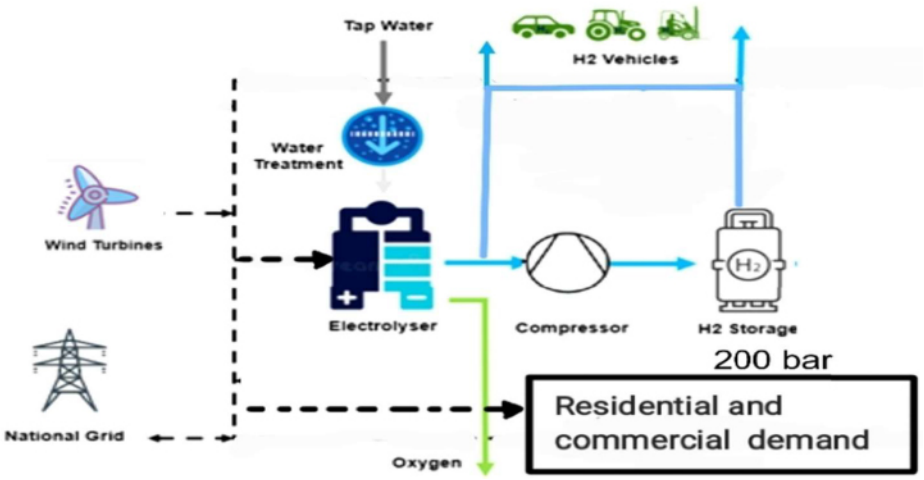

Figure 5. The proposed Wind-H_2 system.

4.1. Calculating the kWh output from the proposed wind turbine

Based on the assessment of several potential development areas (PDA) against several criteria (like terrain, wind speed, noise risk, etc.) as seen in Figure 8, the RINA feasibility study concluded that PDA 3 is the most suitable location for installing the new wind turbine capacity [14]. By matching the HydroGlen feasibility study location picture with Google maps, as illustrated in Figures 6 and 7, PDA 3 was found to be at a latitude of 56.913 and a longitude of −2.551.

Using Global wind Atlas, which is a free, web-based application, the wind speed was found by drawing a 3 km by 3 km rectangular on the PDA 3 location using the webpage map [24]. However, the wind speed was normalized as the result display the wind speed index as shown in Figure 8.

The denormalized wind speed was then calculated by multiplying the monthly wind speed index by the location wind speed which was found by the Global wind Atlas to be 9.81 m/s. Equation (3) [25] was then used to transform the obtained monthly wind speed at reference height of 100 m to the equivalent speed at the new wind turbine target height of 50 m as shown in Table 6.

$$\frac{U(z)}{U(z_r)} = \frac{\ln\left(\frac{z}{z_r}\right)}{\ln\left(\frac{z}{z_0}\right)} \tag{3}$$

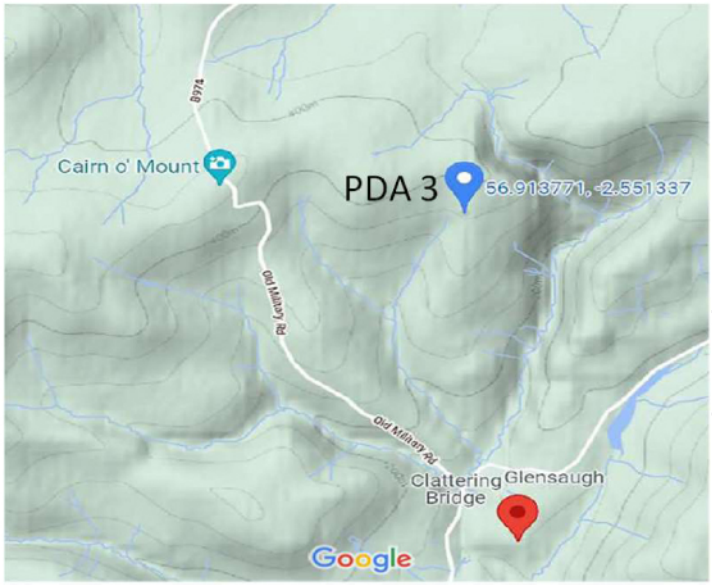

Figure 6. Plot showing the latitude and longitude of PDA 3 using Google maps.

Figure 7. Normalized wind speed at the new turbine location using Global Wind Atlas Online Software.

where, z is the target height (m), z_r is reference height (m), z_o is characteristic terrain length or roughness (m), $U(z)$ is wind velocity at target height z, and $U(z_r)$ is wind velocity at reference height z_r. The characteristic terrain length of the site (z) was found to be 0.03 by using the global wind atlas software, which matches the fallow field's characteristic terrain length in [25].

The wind speed time series (from Table 6) was then merged with the wind turbine power curve (yellow curve) shown in Figure 9 to find the available/theoretical wind power at each speed (P_o), results are shown in Table 7. According to Neill, only part of the available/theoretical power can be harvested by a wind turbine [26]. Therefore, the actual/extracted wind power (P_e)

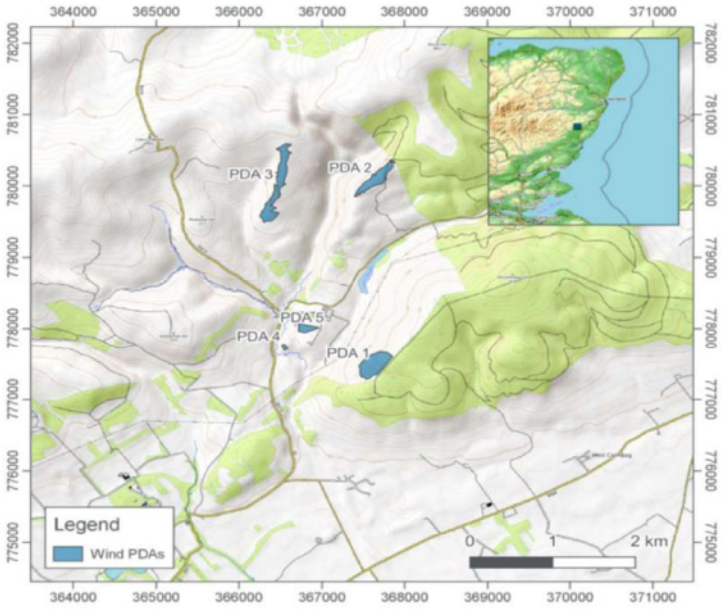

Figure 8. Plot showing the development areas identified within HydroGlen feasibility study as being suitable for wind turbine placement [14].

Table 6. Wind speed calculations at the proposed new turbine height of 50 m.

Month	Monthly wind speed index at height 100 m (normalized wind speed)	Location wind speed (m/s)	Monthly denormalized wind speed at height 100 m ($U(z)$) (m/s)	Monthly wind speed at height 50 m ($U(z_r)$) (m/s)
January	1.21	9.81	11.8701	10.86
February	1.23	9.81	12.0663	11.04
March	1.09	9.81	10.6929	9.78
April	0.87	9.81	8.5347	7.81
May	0.85	9.81	8.3385	7.63
June	0.75	9.81	7.3575	6.73
July	0.78	9.81	7.6518	7.00
August	0.84	9.81	8.2404	7.54
September	0.91	9.81	8.9271	8.16
October	1.03	9.81	10.1043	9.24
November	1.15	9.81	11.2815	10.32
December	1.32	9.81	12.9492	11.84

was calculated using Equation (4) [26]:

$$P_e = C_p * P_o \tag{4}$$

where C_p is the power coefficient which is the overall efficiency of a turbine extracted from Figure 9.

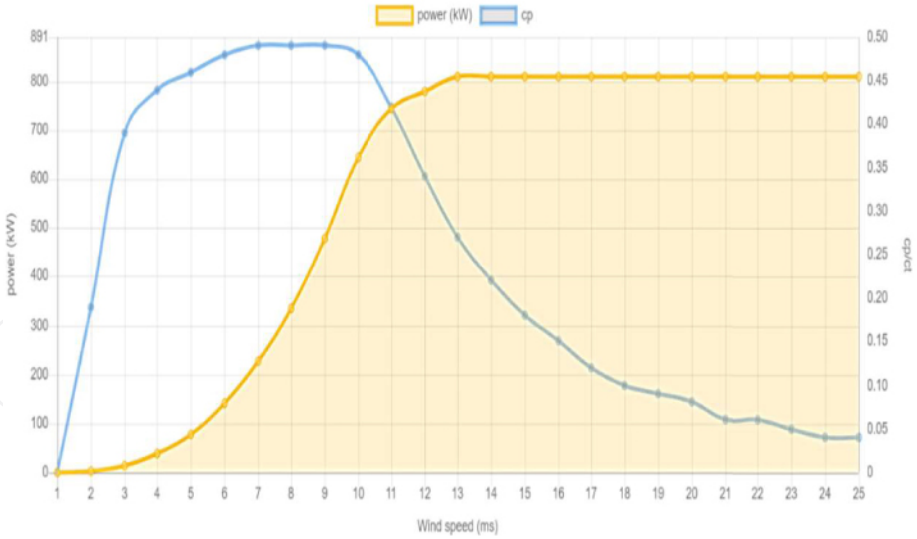

Figure 9. Power curve of Enercon E-53 Wind Turbine [27].

Table 7. Monthly wind energy production and monthly wind energy excess after feeding the residential and commercial total demand.

Month	Monthly wind speed at 50 m height (m/s)	Power coefficient C_p (using the C_p curve in Figure 9)	Wind power P_o (using the power curve in Figure 9) (kW)	Capacity factor C_F	t (hours per month)	Wind production using Equation (5) (kWh)	Monthly residential and commercial demand (kWh)	Monthly wind energy excess after supplying residential and commercial total demand (kWh)
Jan	10.86	0.41	722	0.35	744	77,083.60	43,810	33,273.60
Feb	11.04	0.42	744	0.35	672	73,495.30	35,973	37,522.29
Mar	9.78	0.47	600	0.35	744	73,432.80	37,978	35,454.80
Apr	7.81	0.49	300	0.35	720	37,044	22,330	14,714
May	7.63	0.49	290	0.35	744	37,002.80	23,484	13,518.84
Jun	6.73	0.49	200	0.35	720	24,494.40	20,855	3,639.40
Jul	7.00	0.49	228	0.35	744	29,091.90	18,533	10,558.88
Aug	7.54	0.49	290	0.35	744	37,002.80	19,284	17,718.84
Sep	8.16	0.49	366	0.35	720	45,193.70	19,324	25,869.68
Oct	9.24	0.49	500	0.35	744	63,798	31,548	32,250
Nov	10.32	0.46	672	0.35	720	77,898.20	45,111	32,787.24
Dec	11.84	0.36	790	0.35	744	74,057.80	46,100	27,957.76
Annual						**649,595.35**	364,330	**285,265.35**

The wind output energy was then calculated using Equation (5) [26]:

$$\text{Wind output energy} = P_e * C_F * t \quad (5)$$

where C_F is the capacity factor that describes the relation between the turbine's power output and the maximum power, P_e is actual wind power in kW, and t is

Table 8. Accumulated H_2 calculation results.

Month	Monthly wind energy excess after supplying the residential and the commercial demand (kWh)	Energy consumption of the selected Alkaline electrolyser (kWh/N m³)	Monthly hydrogen production by electrolyser (N m³)	Monthly H_2 consumption for one vehicle (N m³)	No of vehicles that can be supplied by the electrolyser each month	Monthly H_2 excess after supplying the vehicles (N m³)	No of extra vehicles that can be supplied from the accumulated H_2 excess	Monthly accumulated H_2 after feeding the 12 vehicles (N m³)
Jan	33,273.608	5.4	6161.78	473	12	485.78	0	485.78
Feb	37,522.296	5.4	6948.57	473	12	1272.57	0	1758.35
Mar	35,454.8	5.4	6565.70	473	12	889.70	0	**2648.06**
Apr	14,714	5.4	2724.81	473	5	359.81	6	169.87
May	13,518.84	5.4	2503.49	473	5	138.49	0	308.36
Jun	3,639.4	5.4	673.96	473	1	200.96	1	36.32
Jul	10,558.888	5.4	1955.35	473	4	63.35	0	99.67
Aug	17,718.84	5.4	3281.27	473	6	443.27	1	69.94
Sep	25,869.68	5.4	4790.68	473	10	60.68	0	130.62
Oct	32,250	5.4	5972.22	473	12	296.22	0	426.84
Nov	32,787.24	5.4	6071.71	473	12	395.71	0	822.55
Dec	27,957.76	5.4	5177.36	473	10	447.36	2	323.92

number of hours per month. In optimal conditions, a well-designed wind turbine may attain a maximum performance level (C_F) of 35% [28, 29]. Finally, the monthly excess in wind production after feeding the residential and commercial total demand was calculated and results shown in Table 7.

4.2. Sizing the H_2 generator (Electrolyser) based on the excess in wind production

Based on industrial standards, the electrolyser size is often selected to be around (1/3) of the wind capacity [15]. This suggests that for the 800-kW wind capacity a 266.6 kW electrolyser is recommended. For better utilization, three units of 80 kW Hydrogenic HySTAT 15-10 electrolysers were therefore chosen.

4.3. Sizing the storage tank

To size the storage tank, the amount of hydrogen produced by the electrolyser was first calculated based on the surplus wind energy given in Table 7. The previously calculated amount of hydrogen needed for fuelling the farm vehicles was then deducted from the hydrogen produced to find the monthly excess of H_2. Finally, the amount of accumulated hydrogen after supplying the vehicles was calculated to size the storage tank accordingly. Table 8 shows the results for those calculations.

The size of the storage tank is selected based on the maximum amount of accumulated hydrogen which is 2648.06 N m³. Using Boyle's law, the volume of the

needed tank after compression to 200 bars is:

$$V_2 = \frac{10 * 2648.06}{200} = 132.403 \text{ N m}^3.$$

Thus, one storage tank of Hydrogen N5.0 (CP Grade H_2) Manifold cylinder pallet is proposed.

5. LCOE of PV-H_2 and Wind-H_2 systems

The levelized cost of energy (LCOE) was calculated for each of the proposed systems. The LCOE for a renewable source with hydrogen storage is given by Equation (6) [15]:

$$\text{LCOE} = \frac{\sum_{t=1}^{n} \frac{\text{CAPEX}_{\text{RES\&H}_2\text{S},t} + \text{OPEX}_{\text{RES\&H}_2,t}}{(1+r)^t}}{\sum_{t=1}^{n} \frac{\text{E}_{\text{RES},t} + \text{E}_{\text{H}_2,t} + \text{O}_{2,t}}{(1+r)^t}} \quad (6)$$

where Table 9 gives the definition for the equation symbols.

Table 9. LCOE equation symbols definition.

$\text{CAPEX}_{\text{RES\&H}_2,\,t}$ (£)	Capital cost of renewable energy and hydrogen system in year (t)
$\text{OPEX}_{\text{RES\&H}_2,\,t}$ (£)	Operating and maintenance (O&M) cost of renewable system and hydrogen generator in year (t)
r	Discount rate 3% [30]
n	Project lifetime (typically 20 years)
$\text{E}_{\text{Res},\,t}$ (kWh)	Renewable energy output utilised in meeting demands in year (t)
$\text{E}_{\text{H}_2,\,t}$ (kWh)	Energy produced in form of H_2 in year (t)
$\text{O}_{2,\,t}$	Oxygen produced in year (t) ("o" since it was not included in the analysis)

The CAPEX and OPEX of the PV-H_2 system, calculated by adding the costs of all units in the system as shown in Table 10, was found to be £1,332,328 and £5279.59 respectively.

The CAPEX and OPEX of the Wind-H_2 system, calculated by adding the costs of all units in the system as shown in Table 11, was found to be £2,055,894 and £43,141 respectively.

To calculate the LOCE of PV-H_2 and wind H_2 system, the $\text{E}_{\text{Res},\,t}$ (kWh) and $\text{E}_{\text{H}_2,\,t}$ (kWh) (the renewable energy output utilised in meeting demands and the hydrogen production) were first calculated for each of the two systems based on the results in Tables 4 and 7.

The above values were then substituted in Equation (4) along with the CAPEX and OPEX to find the LCOE for each of the proposed systems which were found to be 0.3 £/kWh for the PV-H_2 system and 0.4 £/kWh for the Wind-H_2 system.

Table 10. Estimated CAPEX and OPEX of option (1), the PV-H_2 system components.

Component	Manufacturer	Source	Number of units	Cost per unit	Total cost
CAPEX					
Renesola virtus II 250 W solar PV panels	Renesola	Go GreenMan Solar	2392	£94.74 [31]	£226,618
PV installation			2392	£53 [32]	£126,776
SolarLake 15000TL-PM 15 kW inverter	SamilPower	Renugen	31	£2195.07 [33]	£68,047.17
HyStat-15 electrolyser	Hydrogenics	—	3	£66,964.76 [34]	£200,894.28
Compressor system	Pure Energy Centre	Pure Energy Centre	1	£100,000 [14, 35]	£100,000
Hydrogen storage tank	BOC	BOC	12	£4999.37 [23]	£59,992.42
Hydrogen vehicle refuelling station	—	IRENA	1	£550,000 [14]	£550,000
OPEX					
O&M of PV panels				1% of PV panel cost [36]	£2266.18
O&M of electrolyser				1.5% of electrolyser capital cost [37]	£3013.41

Table 11. Estimated cost of option (2), the Wind-H_2 system components.

Component	Manufacturer	Source	Number of units	Cost per unit	Total cost
CAPEX					
Enercon E53/800 Wind Turbine	Enercon	Go GreenMan Solar	1	£1,003,200	£1,003,200
Wind turbine installation				£196,800 [14]	£196,800
HyStat-15 electrolyser	Hydrogenics		3	£66,964.76 [34]	£200,894.28
Compressor system	Pure Energy Centre	Pure Energy Centre	1	£100,000 [14, 38]	£100,000
Hydrogen storage tank	BOC	BOC	1	£4999.37 [23]	£4999.37
Hydrogen vehicle refuelling station		IRENA	1	£550,000 [14]	£550,000
OPEX					
O&M of wind turbine				4% of wind turbine cost	£40,128
O&M of electrolyser				1.5% of electrolyser cost [37]	£3013.41

Due to the lack of information from Hydrogenic on the cost of the electrolyser, the cost was estimated based on reference [34].

6. Analysis of the proposed hybrid PV-H_2 and Wind-H_2 systems

From Table 4 results, it can be found that the proposed PV system can meet just 35% of the load demand (123,990 kWh/364,350 kWh) because most of the demand is not during the sun availability. Only 21% (123,990 kWh/581,820 kWh) of the total solar energy is being utilized, resulting into around 77% (446,370 kWh/581,820 kWh) of excess in solar energy production (see Table 12). This solar energy excess is stored in the form of green H_2 to be used as clean fuel for the farm's vehicles. On analyzing Table 5 results, it can be found that the proposed HES system was able to meet all the 12 vehicles' transportation demand from March until September. From September to December, all the transportation demand was met after using the stored accumulation of hydrogen from previous months. Although not all the 12 vehicles were supplied in January and February, the accumulated hydrogen after one year will be sufficient to cover these months in the following year. Therefore, it can be concluded that PV-H_2 system is almost capable of meeting 100% of the transport fuel needs by green H_2. Furthermore, after supplying all vehicles, there are still extra H_2 that can be either sold as a commodity or can be converted back to electricity using a fuel cell to feed more residential and commercial demands during the lack of solar energy thus minimising grid imports.

Table 12. Renewable and hydrogen energy outputs of both the PV-H_2 and Wind-H_2 systems.

	PV-H_2 system	**Wind-H_2 system**
E_{Res} (kWh)	123,990	364,330
E_{H_2} (kWh)	133,911	85,580
	(solar energy excess * H_2 RTE)	(wind energy excess * H_2 RTE)

In comparison, it can be concluded from Tables 7 that the proposed Wind-H_2 system can meet almost 100% of the farm's residential and commercial demands by wind energy, and 44% (285,265.35 kWh/649,595.35 kWh) of the wind production is converted to H_2 for vehicles fuelling.

Figure 10 was then constructed using columns 3 and 4 from Tables 4 and column 7 from Table 7 that represent the monthly solar production, the monthly residential and commercial demands, and the monthly wind production respectively to investigate the ability of the PV-H_2 and the Wind-H_2 in meeting residential and commercial demands while producing green H_2 fuel from the excess to powering the transport demands. It can be seen that the wind generation profile closely matches the monthly residential and commercial demand, given the higher demand

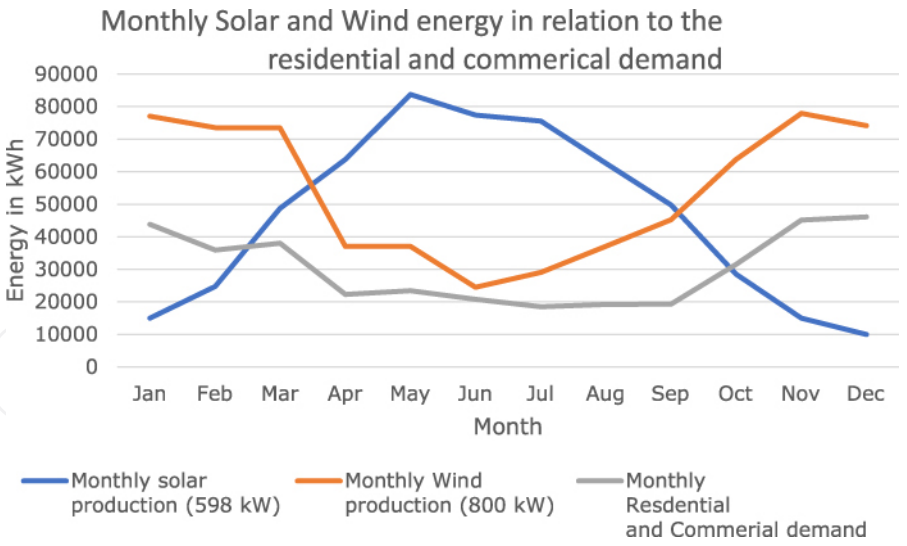

Figure 10. Monthly solar and wind energy production in relation to the residential and commercial demand curve.

in the winter and lower demand in the summer. On the other hand, the Solar profile can be seen out of synchronism with the residential and commercial demand but allows plenty of green H_2 production to be used as fuel for meeting the transport needs as well as being sold as commodity.

From Table 10, it was found that LCOE for the PV-H_2 system is 0.3 £/kWh lower than that of the Wind-H_2 system of 0.4 £/kWh. This implies that the PV-H_2 system is more cost competitive than the wind-H_2 system at current prices, which might be attributed to the wind turbine's high capacity and O&M costs. Reducing the CAPEX and/or increasing the round-trip efficiency of the hydrogen system in the future will allow reducing the LCOE of renewable-H_2 systems to become more financially competitive with other technologies such as natural gas, which is 213 US/MWh [39], this equates to 0.16 £/kWh.

7. Developing a MATLAB/Simulink model for the proposed PV-H_2 system

In order to assess in more detail, the potential of the PV-H_2 system (given that a PV-H_2 system was not considered by RINA), a Simulink model is developed in this section to simulate the generation of the proposed PV system and its overall utilization in the electrolyser to produce green H_2. An electrochemical model has been used to model the electrolyser's green hydrogen production. The developed electrochemical model gives more accurate results as it considers the hydrogen production as function of the current output from the proposed PV system modelled using MATLAB/Simulink, as seen in Figure 11.

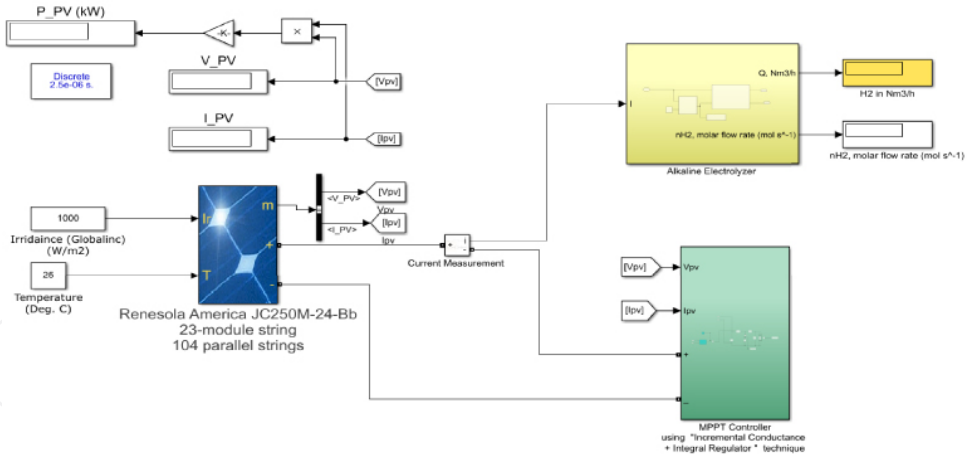

Figure 11. The developed Simulink model for the proposed PV-H_2 system.

The amount of hydrogen produced by the electrolyser is also calculated using the electrolyser's energy consumption calculation method in order to compare the result to the Simulink model results.

7.1. Modelling the proposed PV array

The proposed 598-kW photovoltaic capacity was modelled using the MATLAB/Simulink PV Array block. The PV Array block is a five-parameter model that employs a light-generated current source (IL), a diode, series resistance (Rs), and shunt resistance (Rsh) to simulate the modules' irradiance and temperature-dependent *I–V* characteristics, as seen in Figure 12. The diode *I–V* characteristics for a single module are defined by Equations (7) and (8) [40]:

$$I_d = I_o \left[\exp\left(\frac{V_d}{V_T}\right) - 1 \right] \tag{7}$$

$$V_T = \frac{kT}{q} * nl * N_{\text{cell}} \tag{8}$$

where, all the symbols in Equations (7) and (8) are defined in Table 13.

The PV array block was then modified to model the proposed 598 kW solar capacity. The module was set as RenSola America J250M to be similar to the farm currently installed PV. The PV array block's module parameters were then set to correspond to the PV module parameters listed in the PV datasheet [41]. The parallel strings and series modules were set to 104 and 23, respectively, as determined from the PVsyst simulation results shown in Figure 3. Based on this, the following values resulted for the output voltage and current:

$$I_{\text{PV}} = I_{\text{mp}} \times N_{\text{Parallel string}} = 8.31 * 104 = 864.24 \text{ A} \tag{9}$$

$$V_{\text{PV}} = V_{\text{mp}} \times N_{\text{series modules}} = 30.1 * 23 = 692 \text{ A} \tag{10}$$

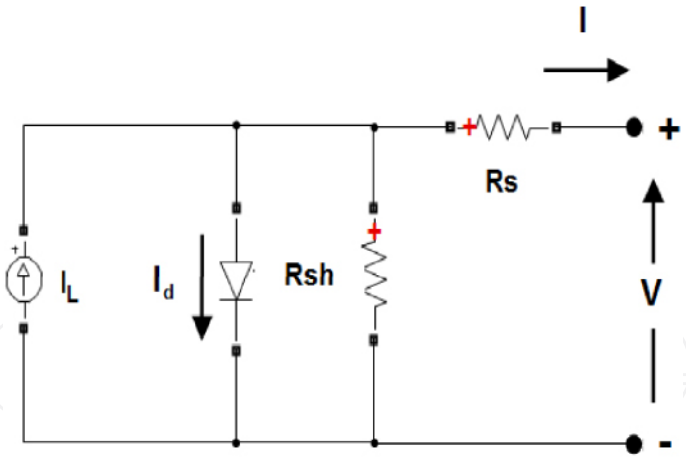

Figure 12. Inner circuit of PV array.

Table 13. Definitions of PV array equation.

I_d	Diode current (A)
V_T	Thermal voltage (V)
V_d	Diode voltage (V)
I_o	Diode saturation current (A)
nI	Diode ideality factor, a number close to 1.0
k	Boltzmann constant = 1.3806×10^{-23} J·K^{-1}
q	Electron charge = 1.6022×10^{-19} C
T	Cell temperature (K)
N_{cell}	Number of cells connected in series in a module

where I_{mp} in (A) and V_{mp} in (V) denote respectively the current and voltage at the maximum power points obtained from the module cell parameters shown in Figure 13. Hence, the maximum power of the PV array is:

$$P_m = I_{mp} \times V_{mp} = 8.31 * 104 = 864.24 * 692 = 598.054 \text{ A}. \quad (11)$$

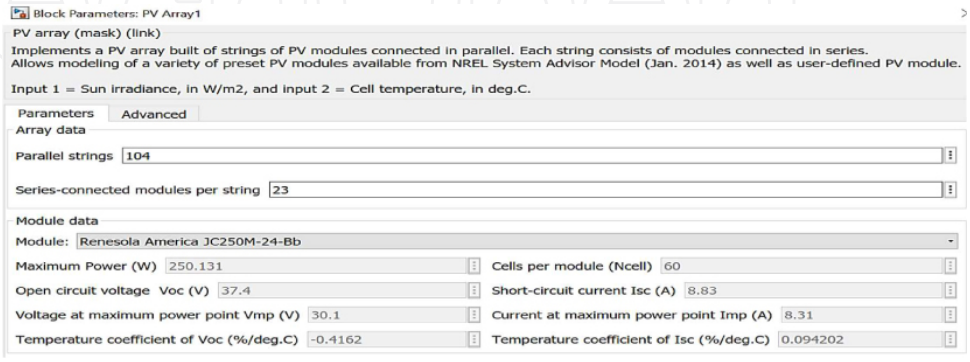

Figure 13. The PV array block with adjusted parameters to meet the proposed PV specifications.

Figure 14 shows the output *I–V* characteristics of the modelled PV array block. It can be seen that, at Standard Test conditions (1000 w/m^2, Cell Temperature 25° C), the array output simulates the 598 kW capacity.

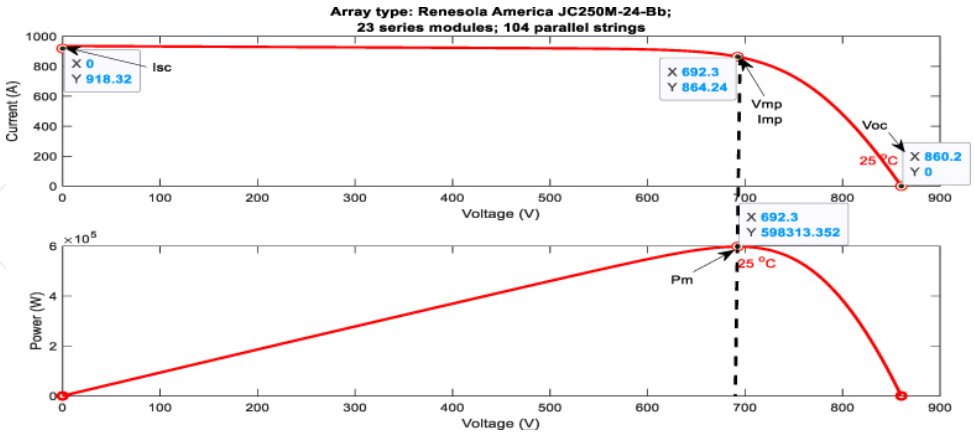

Figure 14. PV array *I–V* characteristics at STC.

To ensure the PV array provides maximum power at all times, an MPPT (Maximum power point tracking) controller with incremental conductance technique block was integrated with the PV array to account for variables such as fluctuating irradiance (sunlight) and temperature [42]. The file exchange of the MPPT block can be found here [43].

7.2. Electrolyser modelling

An Alkaline electrolyzer electrochemical model, as shown in Figure 15, is developed in this section.

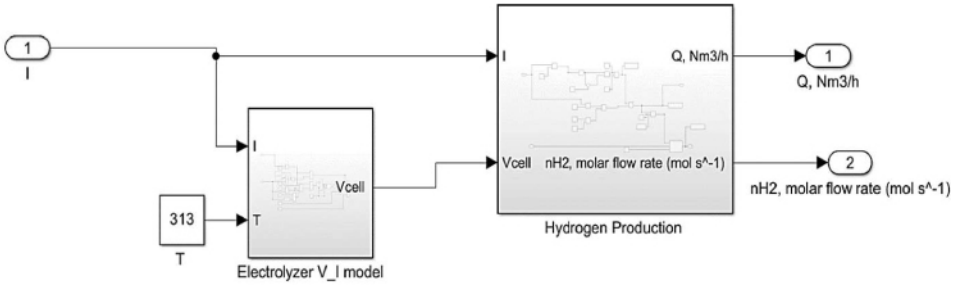

Figure 15. Alkaline electrolyzer block diagram.

7.2.1. Hydrogen production block

The production rate of hydrogen in an alkaline electrolyser is related to the input current as given by Equation (12) [44]:

$$\dot{n}H_2 = \eta F \frac{ncI}{zF} \tag{12}$$

where, nH_2 is the molar flow rate (mol s^{-1}); ηF is the Faraday efficiency; z is 2 (number of electrons transferred per reaction); I is the current (A); F is the Faraday constant 96,485 C mol^{-1}, and nc is the number of series cells in electrolyser cell stack. Since three electrolysers are used (refer to Section 3.2), then nc is 3. Faraday efficiency is given by the Equation (13) [44]:

$$\eta F = \frac{\left(\frac{I}{A}\right)^2}{f_1 + \left(\frac{I}{A}\right)^2} f_2 \tag{13}$$

where, A: is the electrode area (m^2) = 0.25; I: is the current (A); f_1 is Faraday efficiency parameter ($mA^2\ cm^{-4}$) = 150; f_2 is the Faraday efficiency parameter number between 0 and 1 = 0.99, and f_1 and f_2 are selected empirically [44].

The flow rate obtained from Equation (12) is then converted from moles to N m^3/h to facilitate comparison in the results section. The H_2 production in N m^3/h (Q) is given by Equation (14) using the ideal gas volume V_{std} of 0.022414 m^3/mol [44].

$$Q = \dot{n}H_2 * 3600 * 0.022414. \tag{14}$$

A MATLAB/Simulink Hydrogen Production block was then developed as seen in Figure 16 using Equations (12) to (14).

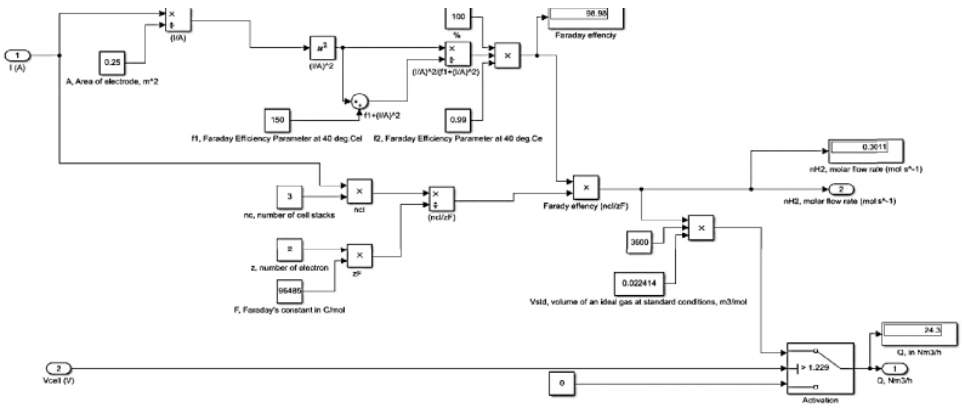

Figure 16. The developed alkaline electrolyser hydrogen production block in MATLAB/Simulink.

7.2.2. Electrolyser V-I model

However, the H_2 production rate obtained by using Equation (12) is independent of the input voltage which is incorrect since water can only split into hydrogen and oxygen when the cell voltage is sufficient to activate this [45]. Thus, the cell voltage is expressed as shown in Equation (15) [44].

$$V_{cell} = V_{rev} + s \log\left(\frac{t_1 + \frac{t_2}{T} + \frac{t_3}{T^2}}{A} I + 1\right) + \frac{r_1 + r_2 T}{A} I \tag{15}$$

where, V_{cell} is the cell voltage (V); V_{rev} is the reversible cell voltage (V); $r_{1,2}$ are the empirical ohmic resistance parameters of electrolyte (Ωm^2); T is the temperature (K); $t_{1,2,3}$ are the empirical overvoltage parameters of the electrode (mA^{-1} m^2); s is the overvoltage parameter of the electrode (V); A is the electrode area (m^2), and I is the current (A). All parameters used in Equation (15) are listed in Table 14 and were obtained from Oystein Ulleberg [44].

Table 14. Alkaline electrolyser constant parameters for Equations (4)–(10) [44].

Symbol	Description	Unit	Value
A	Area of electrode	m^2	0.25
S	Overvoltage parameter of electrode	V	0.185
t_1	Empirical overvoltage parameter of electrode	A^{-1} m^2	1.002
t_2	Empirical overvoltage parameter of electrode	A^{-1} m^2 °C	8.424
t_3	Empirical overvoltage parameter of electrode	A^{-1} m^2 $°C^2$	247.3
r_1	Electrolyte ohmic resistive parameter	Ωm^2	8.05×10^{-5}
r_2	Electrolyte ohmic resistive parameter	Ωm^2 $°C^{-1}$	-2.5×10^{-7}

V_{rev} was then calculated as 1.207 V at an ambient Temperature of 40° C (from datasheet) using the Equation (16) [44]:

$$V_{rev,T(K)} = 1.5184 - 1.5421 \times 10^{-3}T + 9.523 \times 10^{-5}T \ln T + 9.84 \times 10^{-8}T. \quad (16)$$

Equation (15) was then used to develop the Electrolyser V-I block components, as shown in Figure 17.

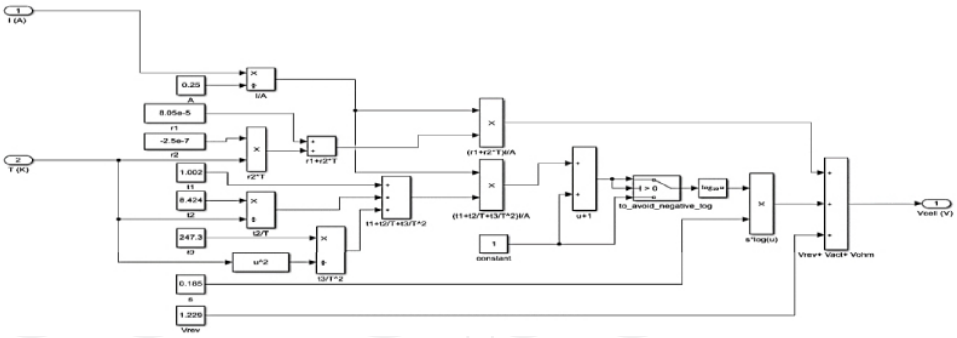

Figure 17. The developed V-I block for alkaline electrolyser in MATLAB/Simulink.

Finally, the boundary condition was added to the developed Hydrogen Production modelling block to allow hydrogen production only when cell voltage is greater than V_{rev}. The complete electrolyser model is shown in Figure 15.

7.3. The MATLAB/Simulink PV-H_2 model results and discussion

To simulate the electrolyser's hourly H_2 output, the hourly solar irradiance and hourly ambient temperature data are required as input to the developed PV array

block. To obtain this data, the PVsyst software was used to generate this hourly data for the 598 kW PV system. PVsyst generates various types of irradiance data, including global irradiation in the horizontal plane (GlobHor), global irradiation in the collector plane (GlobInc), and "Effective" global irradiation on collectors. GlobInc was the one utilised as input for the Simulink PV array block because refers to the total irradiance received ("viewed") by the tilted plane [16].

Table 15 demonstrates some of the findings of the estimated H_2 output derived based on the electrolyser's energy consumption (5.4 kWh/N m^3), versus the estimated H_2 output from the developed Simulink model which is based on the electrolyser electrochemical model.

Table 15. The estimated H_2 output from electrolyser using the electrolyser's energy consumption versus that using the developed Simulink model.

Month/day/hour	Hourly solar irradiance (W/m^2) (GlolbInc using PVsyst)	Hourly T Amb (°C) (using PVsyst)	Hourly DC power from PV (kW) (using PVsyst)	Hourly DC PV power (kW) (using Simulink)	Estimated H_2 output based on the electrolyser's energy consumption and the PVsyst hourly excess power (N m^3 /h)	Estimated H_2 output from the developed Simulink model (N m^3 /h)
Jan/31/13:00	74.38	10.5	41.07	44.75	7.60	8.05
Feb/28/13:00	564.91	12.86	311.54	358	57.69	60
Mar/15/13:00	522.50	8.54	296.02	337	54.81	56.17
Apr/15/13:00	298.69	8.47	171.25	186.32	31.71	34.25
May/15/13:00	719.95	14.01	389.71	435	72.17	79
Jun/15/13:00	683.62	17.35	366.75	421	67.91	75
Jul/15/13:00	384.51	24.90	215.43	227	39.89	42
Aug/15/13:00	790.33	18.79	414.15	417	76.69	87
Sep/15/13:00	326.98	15.7	182.96	201.75	33.88	35.85
Oct/31/13:00	159.85	8.25	91.13	97.5	16.87	17.66
Nov/30/13:00	303.96	7.28	171.72	191	31.8	34.05
Dec/15/13:00	42.76	7.5	21.81	22	4.04	4.5
Dec/31/13:00	192.39	9.1	107.701	119.6	19.94	21.9

The effect of the irradiance and temperature variations on the solar power generation and H_2 production were investigated over different hours of the years. Figure 18 shows the solar power produced from the proposed PV system when using PVsyst simulation versus the Solar power production on using the Simulink model; it can be observed that solar production in summer days is higher than that of winter days as irradiance decreases. It can also be observed that the estimated power generation on using Simulink is higher than that using PVsyst, and this is due to the fact that Simulink model does not account for losses such as soiling loss and wiring loss.

To minimize the number of parameters involved in the electrolyser simulation analysis, a simpler Faraday efficiency equation with non-temperature-dependent

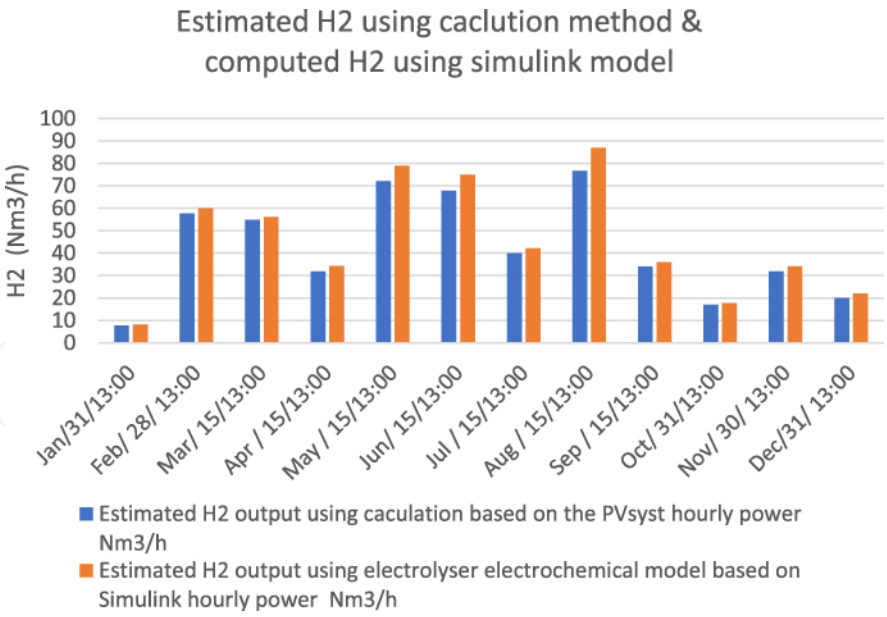

Figure 18. Estimated H_2 based on calculation method and computed-H_2 based on Simulink model.

coefficients (Equation (13)) was utilized. A deeper examination of the hydrogen generation results on accounting for the varying electrical current (the orange bar in Figure 19) reveals that the previously predicted H_2 based on based on the electrolyser's energy consumption (5.4 kWh/N m^3) correspond well with the modelled one and thus validate the calculations undertaken in the design process. However, the H_2 generated by the electrolyser electrochemical model was found slightly more than that produced based on the electrolyser's energy consumption (calculation method), this is because the Simulink model does not account for losses such as soiling loss and wiring loss.

8. Conclusion

Two combinations of Renewable-H_2 energy systems were proposed, sized and assessed in this paper to identify the scenario that meets most of Glensaugh farm residential and commercial demands with green energy as well as providing green H_2 fuel for the farm transport demand. It was found that the proposed grid-connected PV-H_2 system is capable of feeding almost 100% of Glensaugh transportation fuel requirements with green hydrogen and 35% of Glensaugh residential and commercial demands with clean solar energy, with the gird meeting the remaining demands. The proposed wind-H_2 system was found capable of meeting most of the residential and commercial demands by clean wind energy in addition to around 44% of the transport demand by green H_2.

The results obtained for the PV-H_2 system is due to the fact that most of the residential demands are during evenings resulting into a lot of solar daytime energy

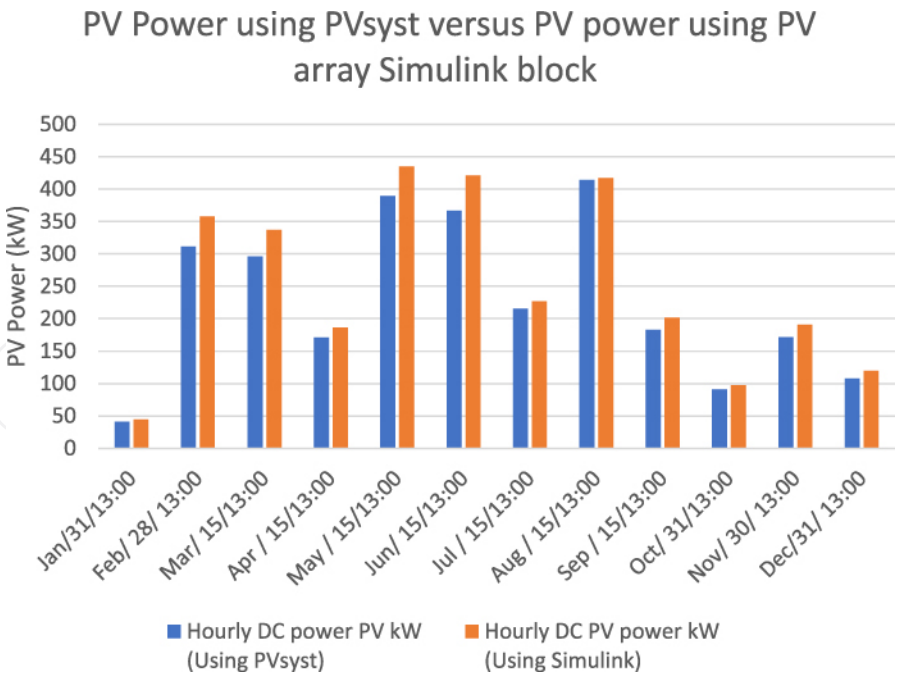

Figure 19. The PV power output using PVsyst versus the PV power output using the developed Simulink model at different hours of the year.

converted to green H_2 for powering the vehicles. The H_2 accumulated after feeding all vehicles could be either sold as a commodity or converted back to electricity by using a fuel cell to feed the residential and commercial demands during the shortage of solar energy, thus improving the overall system efficiency. The results obtained for the wind-H_2 system, on the other hand, is because the wind energy profile is very closely matched with the residential and commercial demand, and thus most wind energy is consumed by this demand, leaving only a small amount of wind energy excess to meet the green H_2 fuel transport demands.

It was also found that the levelized cost of energy of the proposed PV-H_2 system is 0.3 £/kWh, more cost competitive than that of the wind-H_2 of 0.4 £/kWh. On the other hand, the reduction in carbon footprint achieved on using Wind-H_2 system was found higher that of PV-H_2 system. Given that this paper is focusing on assessing the PV-H_2 system, a Simulink model was developed for the PV-H_2 system, and it utilized an electrolyser electrochemical model to model the system green hydrogen production.

Implementing the proposed Renewable-H_2 systems in Scottish farms will provide an excellent opportunity in maximizing the implementation of green energy and green H_2 to meet the current Scottish Government's goal of reaching at least 5 GW of renewable and hydrogen generation by 2030 and at least 25 GW of hydrogen production by 2045 [38]. Developing and promoting such ecologically sustainable

green concepts will be a crucial step in transforming Scottish Farms into an energy-efficient and environmentally sustainable communities.

For future work, it is recommended to investigate a renewable energy mix scenario, with wind and solar employed together to reduce the grid import and meet the transport fuel demand by green H_2. Wind energy may be sized to meet the commercial and residential demand since its generation profile closely matches the monthly consumption. At the same time, a solar-hydrogen system could be employed to meet the transportation demand fuel needs and the excess in green H_2 to be sold as a commodity. Furthermore, the system can be investigated with a grid connection import/export capacity to facilitate additional revenue through grid export.

It is also recommended to investigate the sale of the O_2 produced by the electrolyser as a commodity to increase the system economic efficiency (overall competitive value) of the system.

To allow investigating a large number of data such as examining the variation of irradiance every hour of the year, it is suggested to use a strain generator rather than a constant block to allow input a series of irradiance data. This could be more efficient. Further research into the impact of thermal transients in electrolysers could also be investigated.

Conflict of interest

The authors declare no conflict of interest.

Acknowledgements

The data and feasibility reports used for this case study have been provided by the James Hutton Institute (JHI).

References

1 López González E, Isorna Llerena F, Silva Pérez M, Rosa Iglesias F, Guerra Macho J. Energy evaluation of a solar hydrogen storage facility: comparison with other electrical energy storage technologies. *Int J Hydrogen Energy*. 2015 Apr;**40**(15):5518–5525. doi:10.1016/j.ijhydene.2015.01.181.

2 Chen H, Xu Y, Liu C, He F, Hu S. Storing energy in China–an overview. In: *Storing energy*. Amsterdam: Elsevier; 2016. p. 509–527. doi:10.1016/B978-0-12-803440-8.00024-5.

3 Mahmoud D, Ali M. Hydrogen energy storage. In: *Energy storage devices [Internet]*. IntechOpen; 2019. Available from: www.intechopen.com, doi:10.5772/intechopen.88902.

4 Widera B. Renewable hydrogen implementations for combined energy storage, transportation and stationary applications. In: *Thermal science and engineering progress*, vol. 16, Amsterdam: Elsevier; 2020 May. doi:10.1016/j.tsep.2019.100460.

5 Melaina M, Eichman J. *Hydrogen energy storage: grid and transportation services (Technical Report)*. Golden, CO (United States), 2015 Feb. doi:10.2172/1170355.

6 Lee DY, Elgowainy A, Kotz A, Vijayagopal R, Marcinkoski J. Life-cycle implications of hydrogen fuel cell electric vehicle technology for medium- and heavy-duty trucks. *J Power Sources*. 2018 Jul;**393**: 217–229. doi:10.1016/j.jpowsour.2018.05.012.

7 Astiaso Garcia D. Analysis of non-economic barriers for the deployment of hydrogen technologies and infrastructures in European countries. *Int J Hydrogen Energy*. 2017 Mar;**42**(10):6435–6447. doi:10.1016/j.ijhydene.2017.01.201.

8 Castañeda M, Fernández LM, Sánchez H, Cano A, Jurado F. Sizing methods for stand-alone hybrid systems based on renewable energies and hydrogen. In: *Proceedings of the Mediterranean Electrotechnical Conference – MELECON*. Piscataway, NJ: IEEE; 2012. p. 832–835. doi:10.1109/MELCON.2012.6196558.

9 Hossain KK, Jamal T. Solar PV-hydrogen fuel cell system for electrification of a remote village in Bangladesh. In: *Proceedings of 2015 3rd International Conference on Advances in Electrical Engineering, ICAEE 2015*. Piscataway, NJ: IEEE; 2016 Jul. p. 22–25. doi:10.1109/ICAEE.2015.7506787.

10 Bernoosi F, Nazari ME. Optimal sizing of hybrid PV/T-fuel cell CHP system using a heuristic optimization algorithm. In: *34th International Power System Conference, PSC 2019*. Piscataway, NJ: IEEE; 2019 Dec. p. 57–63. doi:10.1109/PSC49016.2019.9081541.

11 Daraei M, Campana PE, Thorin E. Power-to-hydrogen storage integrated with rooftop photovoltaic systems and combined heat and power plants. *Appl Energy*. 2020 Oct;**276**. 115499, doi:10.1016/j.apenergy.2020.115499.

12 Simonis B, Newborough M. Sizing and operating power-to-gas systems to absorb excess renewable electricity. *Int J Hydrogen Energy*. 2017 Aug;**42**(34):21635–21647. doi:10.1016/j.ijhydene.2017.07.121.

13 McDonagh S, Ahmed S, Desmond C, Murphy JD. Hydrogen from offshore wind: investor perspective on the profitability of a hybrid system including for curtailment. *Appl Energy*. 2020 May;**265**. 114732, doi:10.1016/j.apenergy.2020.114732.

14 RINA. *A non-technical summary of the HydroGlen project feasibility study [Internet]*. 2021 March [cited 2022 Mar 7]. Aberdeen: James Hutton Institute; 2021. Available from: https://www.hutton.ac.uk/sites/default/files/files/publications/Glensaugh_HydroGlen_NonTech_Feasibility_March2021.pdf.

15 Gazey RN. Sizing hybrid green hydrogen energy generation and storage systems (HGHES) to enable an increase in renewable penetration for stabilising the grid [thesis]. Aberdeen (UK): Robert Gordon University; 2014.

16 Mermoud A, Wittmer B. *PVsyst user's manual PVsyst SA-route du [Internet]*. Switzerland: PVsyst SA; 2014. Available from: www.pvsyst.com.

17 Madhumitha J. Total monthly hours of sunlight in the United Kingdom (UK) from 2014 to 2020 [Internet]. *Statista*. 2021 Nov 08 [cited 2021 Nov 17]. Available from: https://www.statista.com/statistics/584898/monthly-hours-of-sunlight-in-uk/.

18 Franklin EA. *Calculations for a grid-connected solar energy system*. Tucson, AZ: University of Arizona Cooperative Extension; 2019. p. 2–6.

19 Thomas D. *State of play and developments of power-to-hydrogen technologies [Internet]*. 2019 [cited 2022 Jan 23]. Available from: https://etipwind.eu/wp-content/uploads/A2-Hydrogenics_v2.pdf.

20 Fordham M. *Photovoltaics and architecture*. In: Thomas R, editor. London: Spon; 2000.

21 Bernier E, Hamelin J, Agbossou K, Bose TK. Electric round-trip efficiency of hydrogen and oxygen-based energy storage. *Int J Hydrogen Energy*. 2005 Feb;**30**(2):105–111. doi:10.1016/j.ijhydene.2004.03.039.

22 Pure Energy Centre. *Pure H_2 hydrogen compressors [Internet]*. 2021 [cited 2022 Feb 18]. Available from: https://pureenergycentre.com/hydrogen-compressor/.

23 BOC. Hydrogen N5.0 (CP grade H_2), BS4, 15 × 50 litre (WL size), steel cylinder MCP, 200 bar – size WL (132m3) [Internet]. *BOC*. 2022 [cited 2022 Feb 04]. Available from: https://www.boconline.co.uk/shop/en/uk/wl-200bar-hydrogen–cp-grade-mcp-290627-wl.

24 Global Wind Atlas. 2022 [cited 2022 Jun 24]. Available from: https://globalwindatlas.info/.

25 Manwell JF, McGowan JG, Rogers AL. *Wind energy explained theory, design and application*. Chichester: Wiley; 2002.

26 Neill SP, Hashemi MR. Offshore wind. *Fundamentals of ocean renewable energy*. Amsterdam: Elsevier; 2018. p. 83–106. doi:10.1016/b978-0-12-810448-4.00004-5.

27 Silvio M, Lucas B. *Enercon E-53 [Internet]*. 2022 [cited 2022 Jan 29]. Available from: https://en.wind-turbine-models.com/turbines/530-enercon-e-53.

28 Elliott D, Infield D. An assessment of the impact of reduced averaging time on small wind turbine power curves, energy capture predictions and turbulence intensity measurements. *Wind Energy*. 2014 Feb;**17**(2):337–342. doi:10.1002/we.1579.

29 Boccard N. Capacity factor of wind power realized values vs. estimates. *Energy Policy*. 2009 Jul;**37**(7):2679–2688. doi:10.1016/j.enpol.2009.02.046.

30 Khatib H. A review of the IEA/NEA projected costs of electricity – 2015 edition. *Energy Policy*. 2016 Jan;**88**: 229–233. doi:10.1016/j.enpol.2015.10.030.

31 Go GreenMan Solar. *ReneSola JC250M-24/Bb-B 250 Watts solar panel [Internet]*. 2022 [cited 2022 Mar 12]. Available from: https://gogreenmansolar.com/product/renesola-jc250m-24-bb-b-250-watts-solar-panel/.

32 Hassan A, Saadawi M, Kandil M, Saeed M. Modified particle swarm optimisation technique for optimal design of small renewable energy system supplying a specific load at Mansoura University. In: *IET renewable power generation*. Hoboken, NJ: Wiley Online Library; 2015 Jul. p. 474–483. doi:10.1049/iet-rpg.2014.0170.

33 renugen. *Samil SolarLake 15000TL-PM 15 kW three phase inverter [Internet]*. Sevenoaks: Renugen; 2022 [cited 2022 Mar 12]. Available from: https://www.renugen.co.uk/samil-solarlake-15000tl-pm-15kw-three-phase-inverter/.

34 Bertuccioli L, Chan A, Hart D, Lehner F, Madden B, Standen E. Development of water electrolysis in the European Union. In: *Final Report. Fuel Cells and Hydrogen Joint Undertaking [Internet]*. Cambridge, UK, Lausanne (CH); 2014. Available from: www.e4tech.com.

35 Pure Energy Centre. *Pure N2 compressor [Internet]*. 2022 [cited 2022 Mar 12]. Availabe from: https://pureenergycentre.com/nitrogen-products-pure-energy-centre/nitrogen-compressor/.

36 Lugo-laguna D, Arcos-Vargas A, Nuñez-hernandez F. A European assessment of the solar energy cost: key factors and optimal technology. *Sustainability (Switzerland)*. 2021 Mar;**13**(6):3238. doi:10.3390/su13063238.

37 Lazard. Lazard's levelized cost of hydrogen analysis-executive summary overview of analysis; 2021. Available from: https://www.lazard.com/media/erzb5rkv/lazards-levelized-cost-of-hydrogen-analysis-version-20-vf.pdf.

38 Wheelhouse P. Developing Scotland's hydrogen economy: statement by the Energy Minister [Internet]. *Scotish government*. 2021 Feb 11 [cited 2022 Mar 13]. Available from: https://www.gov.scot/publications/ministerial-statement-developing-scotlands-hydrogen-economy/.

39 Breeze P. The cost of electricity. In: *The cost of electricity*. Amsterdam: Elsevier; 2021. p. 117–136. doi:10.1016/b978-0-12-823855-4.00009-7.

40 MathWorks. PV array [Internet]. *MathWorks*. 2022 [cited 2022 Feb 4]. Available from: https://uk.mathworks.com/help/physmod/sps/powersys/ref/pvarray.html.

41 RenSola. *Virtus ® II Module [Internet]*. 2012 [cited 2022 Feb 25]. Available from: https://s3.us-east-2.amazonaws.com/legacy.portalsolar.com.br/Content/EditorImages/files/ReneSola%20-%20Modelo%20JC260M-24Bb%20-%20260Watts.pdf.

42 MathWorks. *MPPT algorithm [Internet]*. 2022 [cited 2022 Mar 11]. Available from: https://uk.mathworks.com/solutions/power-electronics-control/mppt-algorithm.html.

43 MathWorks. *Detailed model of a 100-kW grid-connected PV array [Internet]*. 2022 [cited 2022 Mar 11]. Available from: https://uk.mathworks.com/help/physmod/sps/ug/detailed-model-of-a-100-kw-grid-connected-pv-array.html.

44 Ulleberg O. Modeling of advanced alkaline electrolyzers: a system simulation approach. *Int J Hydrogen Energy*. 2003 Jan;**28**(1):21–33. doi:10.1016/S0360-3199(02)00033-2.

45 Martinez D, Zamora R. MATLAB simscape model of an alkaline electrolyser and its simulation with a directly coupled PV module. *International Journal of Renewable Energy Research*. 2018 Jan;**8**(1):552–560.